Rapid subsurface warming and circulation changes of Antarctic coastal waters by poleward shifting winds

Paul Spence[1,2], Stephen M. Griffies[3], Matthew H. England[1,2], Andrew McC. Hogg[4], Oleg A. Saenko[5], and Nicolas C. Jourdain[2,6]

[1]ARC Centre of Excellence for Climate System Science, University of New South Wales, Sydney, New South Wales, Australia, [2]Climate Change Research Centre, University of New South Wales, Sydney, New South Wales, Australia, [3]NOAA Geophysical Fluid Dynamics Laboratory, Princeton, New Jersey, USA, [4]ARC Centre of Excellence for Climate System Science and Research School of Earth Sciences, Australian National University, Canberra, Australian Capital Territory, Australia, [5]Canadian Centre for Climate Modelling and Analysis, Environment Canada, Victoria, British Columbia, Canada, [6]Laboratoire de Glaciologie et Géophysique de l'Environnement, Université de Grenoble/Centre National de la Recherche Scientifique, Grenoble, France

Abstract The southern hemisphere westerly winds have been strengthening and shifting poleward since the 1950s. This wind trend is projected to persist under continued anthropogenic forcing, but the impact of the changing winds on Antarctic coastal heat distribution remains poorly understood. Here we show that a poleward wind shift at the latitudes of the Antarctic Peninsula can produce an intense warming of subsurface coastal waters that exceeds 2°C at 200–700 m depth. The model simulated warming results from a rapid advective heat flux induced by weakened near-shore Ekman pumping and is associated with weakened coastal currents. This analysis shows that anthropogenically induced wind changes can dramatically increase the temperature of ocean water at ice sheet grounding lines and at the base of floating ice shelves around Antarctica, with potentially significant ramifications for global sea level rise.

1. Introduction

Antarctic coastal waters are characterized by a subsurface density gradient between cold, relatively fresh waters on the continental shelf and warmer, saltier waters found further offshore [*Jacobs*, 1991]. The deepening of isopycnals toward the Antarctic coast, known as the Antarctic Slope Front, acts as a dynamical barrier to the exchange of heat, salt, and nutrients across the continental shelf [*Jacobs*, 1991; *Smedsrud et al.*, 2006]. Prevailing easterly coastal winds (which induce coastal downwelling) help to maintain the Antarctic Slope Front; the associated subsurface meridional density gradient forms the westward flowing Antarctic Coastal and Slope Currents. The coastal currents and the Antarctic Slope Front are near circumpolar, extending from roughly the Amundsen Sea (120°W) westward to the tip of the Antarctic Peninsula (55°W) [*Whitworth et al.*, 1998]. The dynamical interplay between coastal winds, coastal currents, and heat transport across the Antarctic Slope Front may thus play a crucial role in global sea level rise by influencing mass loss from Antarctic glacial ice sheets [*Mayewski et al.*, 2009].

The intrusion of warm ocean water onto the Antarctic continental shelf causes increased melt rates at the base of floating ice shelves, a retreat of ice sheet grounding lines, and increased ice sheet discharge [*Rignot et al.*, 2004; *Pritchard and Vaughan*, 2007; *Pritchard et al.*, 2012]. Satellite observations of West Antarctica between 1992 and 2006 reveal a 59% increase in the rate of ice mass loss along the Bellingshausen and Amundsen seas and a 140% increase on the western side of the Antarctica Peninsula [*Rignot et al.*, 2008]. The melt rates have a strong positive correlation with ocean thermal forcing: a 1°C increase in ocean temperatures is suggested to increase basal melt rates by ~10 m/yr [*Rignot and Jacobs*, 2002]. There is growing concern that glacial ice sheets can rapidly become unstable, particularly where warmer ocean water interacts with ice sheet grounding lines [*Rignot et al.*, 2004; *Pritchard and Vaughan*, 2007; *Schoof*, 2007].

The scarcity of Antarctic coastal ocean observations, particularly of subsurface properties during the austral winter season, limits direct observational analysis of variability and change [*Mayewski et al.*, 2009]. Here we use a mesoscale eddy-permitting ocean model to investigate the magnitude and causes of subsurface Antarctic coastal ocean variability on decadal time scales. A first experiment investigates the effect of recent atmospheric trends on the Antarctic coastal ocean, and a second experiment focuses on the effect of projected 21st century Southern Ocean wind changes.

2. Methods

2.1. The Ocean-Sea Ice Model

Our primary tool is a global ocean-sea ice model (GFDL-MOM025) that is based on the Geophysical Fluid Dynamics Laboratory (GFDL) CM2.5 coupled climate model [*Delworth et al.*, 2012]. GFDL-MOM025 has a 1/4° Mercator horizontal resolution with ~11 km grid spacing at 65°S. The Antarctic Slope Front and coastal currents typically have widths of ~50 km, except in regions of particularly steep bathymetry (e.g., Ross Sea) where the observed horizontal scale is reduced to ~20 km [*Chavanne et al.*, 2010; *Jacobs*, 1991]. GFDL-MOM025 has 50 vertical levels and is coupled to the GFDL Sea Ice Simulator model. Sea surface salinity is restored to seasonally varying climatology on a 60 day time scale. The model does not have ice cavities.

The GFDL-MOM025 atmospheric state is prescribed and converted to ocean surface fluxes by bulk formulae; consequently, the model does not resolve air-sea feedbacks. The atmospheric forcing is derived from version 2 of the Coordinated Ocean-ice Reference Experiments (CORE) data [*Griffies et al.*, 2009; *Large and Yeager*, 2009].

2.2. Experimental Design

2.2.1. Interannually Varying Atmospheric Forcing

In the first experiment, GFDL-MOM025 was integrated through six cycles of 1948–2007 CORE Inter-Annual Forcing (CORE-IAF) provided at 6 h intervals. We analyze decadal averages from 1958 to 1967 and 1998 to 2007 in the last forcing cycle.

The 1948–2007 atmospheric state includes several observed decadal trends with links to Antarctic coastal ocean variability. First, increased Antarctic Peninsula surface air temperatures since the 1950s [*Chapman and Walsh*, 2007; *Turner et al.*, 2005] (Figure S1a) are associated with warmer near-surface waters in summer on the western side of the peninsula but with little observed impact below 100 m [*Meredith and King*, 2005]. Second, a positive trend in the Southern Annular Mode, associated with strengthened and poleward-shifted southern hemisphere midlatitude westerly winds since the 1950s [*Thompson and Solomon*, 2002] (Figure S1b), may aid the intrusion of water onto the Antarctic continental shelf [*Chavanne et al.*, 2010; *Wåhlin et al.*, 2010; *Hellmer et al.*, 2012], alter sea ice extent and thickness [*Bintanja et al.*, 2013], and impact dense water formation and transport [*Spence et al.*, 2014]. Last, increased Southern Ocean precipitation and glacial runoff can inhibit the vertical mixing of cold surface waters with the underlying warmer waters [*Bintanja et al.*, 2013] and are linked with freshening Southern Ocean water masses [*Rintoul*, 2007; *Durack and Wijffels*, 2010]. However, the Southern Ocean precipitation trends are weak in CORE-IAF (Figure S1c), and observations of Antarctic coastal runoff insufficient to include it in the 1948–2007 model forcing, so runoff is held constant.

2.2.2. Idealized Wind Forcing

The observed Southern Annular Mode trend is consistently projected to persist through the 21st century due to continued anthropogenic forcing [*Fyfe et al.*, 2007; *Zheng et al.*, 2013]. We isolate the impact of the projected 21st century Southern Annular Mode trend on the Antarctic coastal ocean in a series of idealized perturbed Southern Ocean wind simulations initiated from a control GFDL-MOM025 simulation (CNTRL). CNTRL is equilibrated for 100 years under CORE Normal Year Forcing (CORE-NYF). CORE-NYF provides a 1 year climatological mean atmospheric state at 6 h intervals, along with representative synoptic variability [*Large and Yeager*, 2009].

In simulations denoted as $W_{4°S}$, $W_{+15\%}$, and $W_{4°S+15\%}$ the CORE-NYF 10 m winds between 25°S and 70°S are shifted to 4°S, increased in magnitude by 15%, or both (Figure S2). Simulations denoted as $W_{4°S\ (62°S-70°S)}$, $W_{4°S+15\%\ (62°S-70°S)}$, and $W_{4°S+15\%\ (62°S-80°S)}$ have reduced latitudinal ranges (i.e., 62°S–70°S and 62°S–80°S) of perturbed wind forcing. The northern tip of the Antarctic Peninsula is near 62°S. Both meridional and zonal wind components are modified to prevent unrealistic decomposition of the CORE synoptic variability. Smoothing is applied within the 5° latitude of the perturbation boundaries. Anomalies are determined by differencing perturbed simulations from the concomitantly extended CNTRL simulation, with this approach acting to remove effects from model drift.

The idealized wind perturbation scenarios were guided by an assessment of the late 21st century change in Southern Ocean zonal winds induced by "business as usual" anthropogenic forcing (RCP8.5) in 32 climate models from the Fifth Coupled Model Intercomparison Project (CMIP5) (Figure S3; see also *Fyfe et al.* [2007] and *Zheng et al.* [2013]). The barycenter of westerly winds south of 20°S is shifted 3.6°S in the idealized GFDL-MOM025 wind shift scenarios. Twenty-five percent of the CMIP5 models analyzed have a mean barycenter shift of 2.9°S, and three models have a more southward barycenter shift than in our idealized approach. We avoid using CMIP5
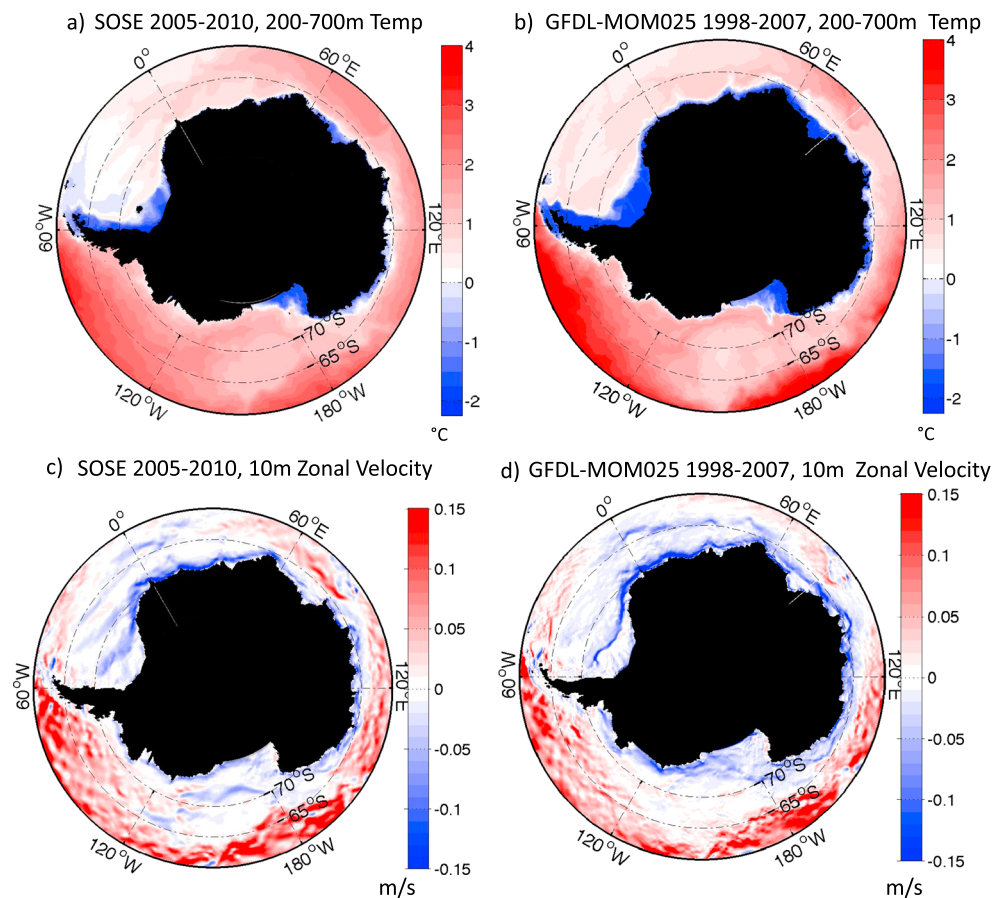
Figure 1. Geophysical Fluid Dynamics Laboratory-Modular Ocean Model (GFDL-MOM025) integrated with 1948–2007 interannually variable atmospheric state compared with Southern Ocean State Estimate (SOSE). (a) SOSE average ocean temperature (°C) between 200 and 700 m depth and years 2005–2010. (b) GFDL-MOM025 1998–2007 average ocean temperature (°C) between 200 and 700 m depth. (c) SOSE years 2005–2010 average ocean zonal velocity (m/s) at 10 m depth. (d) GFDL-MOM025 1998–2007 average ocean zonal velocity (m/s) at 10 m depth.

model mean wind anomalies as forcing due to their equatorward Southern Ocean westerly wind position bias relative to reanalysis data (Figure S3; see also *Swart and Fyfe* [2012]).

As the westerly winds shift poleward under anthropogenic forcing they reduce the meridional extent and strength of the polar easterlies (Figure S3). The transition from zonal average easterly winds to zonal average westerly winds, which occurs at roughly 65°S in CNTRL, is shifted 4°S in the idealized wind forcing simulations. In the CMIP5 models analyzed the transition to zonal average easterly winds is shifted 2.5°S ± 0.5°S for the 32 multi-model ensemble mean, and 4.5°S ± 0.5°S for 25% of the models (Figure S3). The zonal average wind speed anomaly averaged between 65°S and 70°S for the $W_{4°S\ (62°S–70°S)}$ simulation is 1.44 m/s (positive westward), while it is 0.81 m/s for the 32 CMIP5 model ensemble mean and 1.38 m/s for top 25% of the models (Figure S3).

The idealized wind forcings are applied as a consistent anomaly to the CORE-NYF forcing atmospheric state, and as such they do not properly account for temporal or spatial variations of the projected SAM trend. In particular, the observed spatial pattern of the SAM during summer is largely zonally symmetric, and in winter it exhibits increased zonal wave number 2–3 variability [*Codron*, 2005, 2007]. While observational data identify that the largest SAM trend has occurred during spring/summer in recent decades [*Marshall*, 2003], in the future the SAM is projected to trend across all seasons as greenhouse gases take over from ozone depletion as the primary driver of a midlatitude jet shift in the Southern Hemisphere [*Thompson et al.*, 2011].
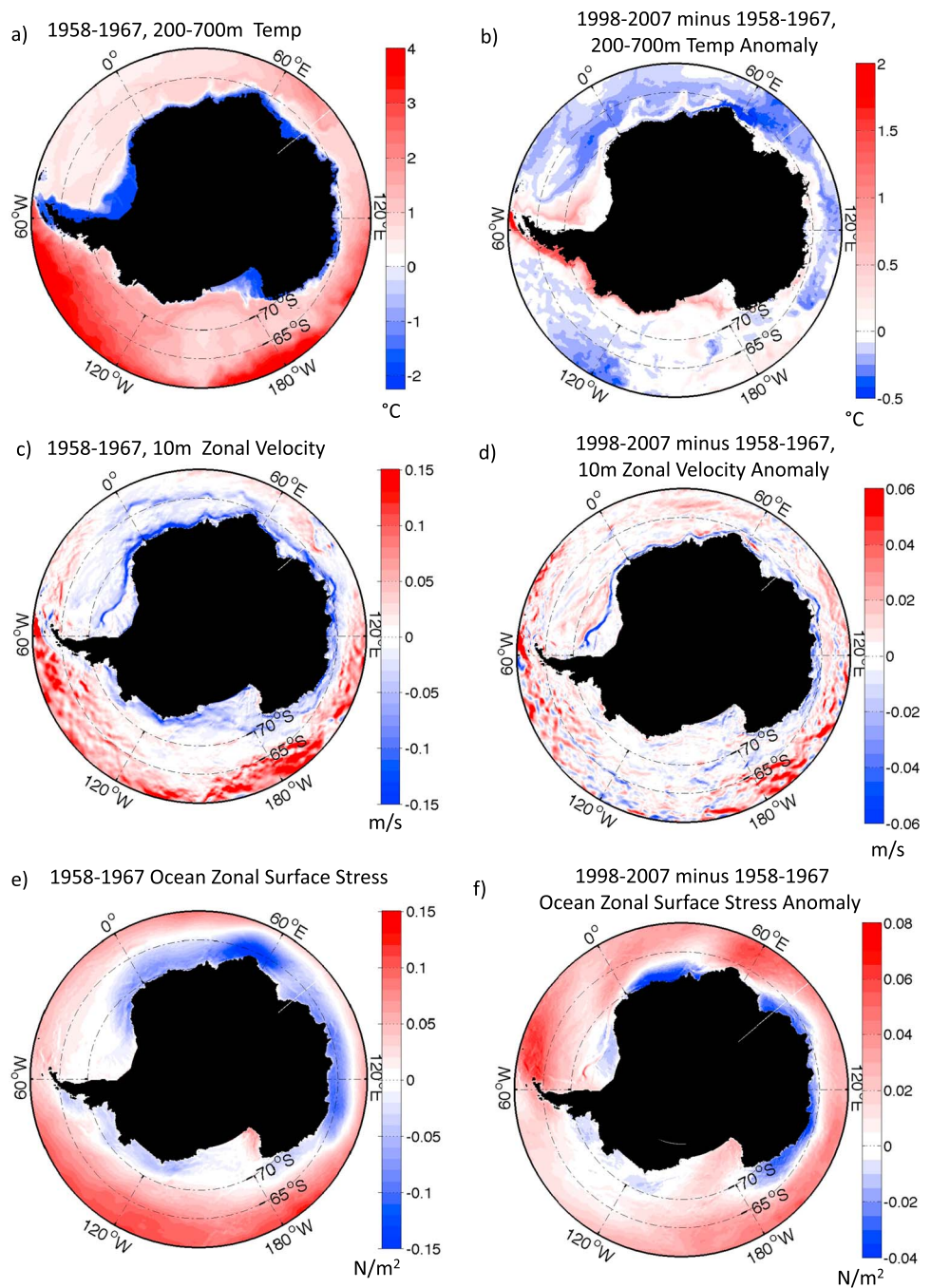
Figure 2. GFDL-MOM025 integrated with 1948–2007 interannually variable atmospheric state. (a) 1958–1967 and (b) 1998–2007 minus 1958–1967 average ocean temperature (°C) between 200 and 700 m depth. (c) 1998–2007 and (d) 1998–2007 minus 1958–1967 average ocean zonal velocity (m/s) at 10 m depth. Note that the zonal velocity structures shown in Figures 2c and 2d are weaker but remain consistent when depth averaged over the upper 700 m. (e) 1958–1967 and (f) 1998–2007 minus 1958–1967 average zonal ocean surface stress (N/m²). (g) 1958–1967 average and (h) 1998–2007 minus 1958–1967 average vertical velocities (m/day, positive upward) due to Ekman pumping. (i) 1958–1967 and (j) 1998–2007 minus 1958–1967 average precipitation minus evaporation plus river runoff freshwater flux (kg/m²/s). Note that the coastal runoff is held constant.

g) 1958-1967 Ekman Pumping

h) 1998-2007 minus 1958-1967
2007 Ekman Pumping Anomaly

i) 1958-1967 Precip minus Evap plus Runoff

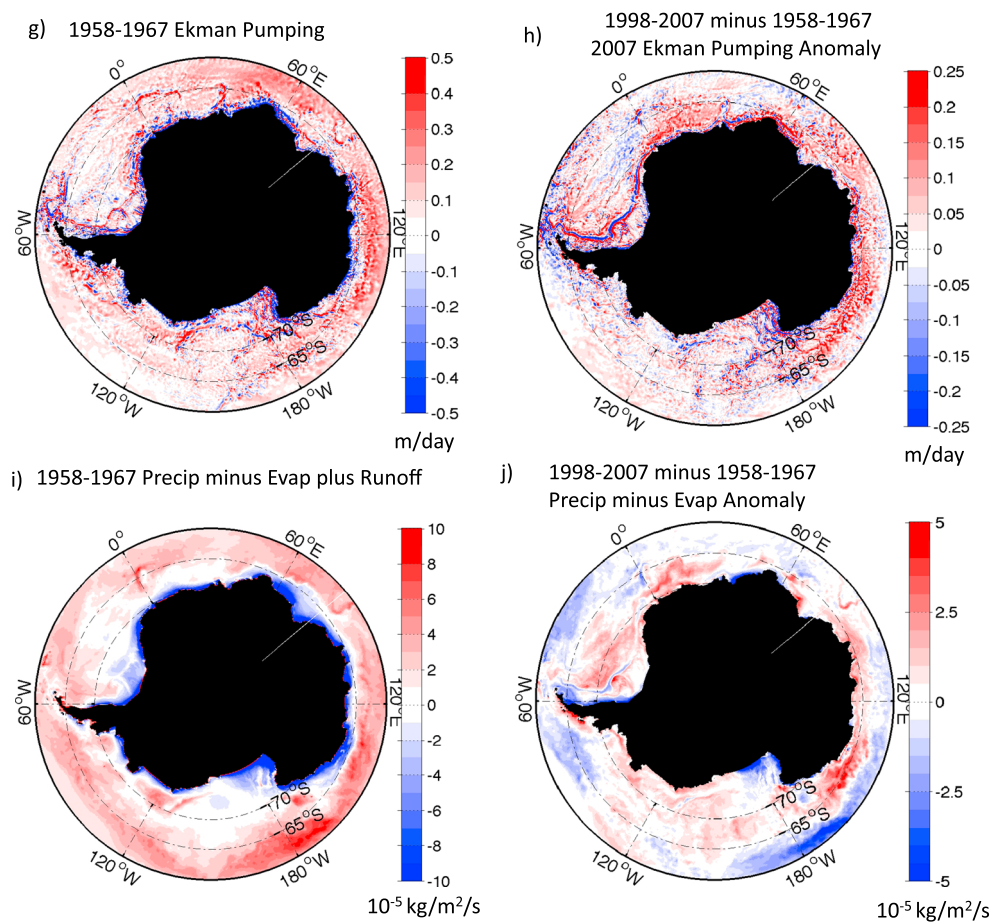j) 1998-2007 minus 1958-1967
Precip minus Evap Anomaly

Figure 2. (continued)

3. Results

3.1. Interannually Varying Atmospheric Forcing Response

To evaluate Antarctic coastal ocean properties in GFDL-MOM025 we use the 1/6° horizontal resolution Southern Ocean State Estimate (SOSE), which is optimized to match available ocean observations spanning years 2005–2010 [*Mazloff et al.*, 2010]. The lack of winter season observations, particularly in the sea ice-covered Antarctic coastal region, may provide a bias in SOSE. When evaluated over similar years, SOSE and the interannually forced GFDL-MOM025 simulations have remarkably similar subsurface coastal ocean temperature and zonal velocity structures (Figure 1). This agreement includes weaker offshore temperature gradients and coastal currents west of the Antarctic Peninsula, from roughly 65°W westward to 120°W, relative to other Antarctic coastal regions. The primary differences between the model and the SOSE reanalysis are the more extensive cold water regions along the continental shelf and more intense coastal currents in GFDL-MOM025.

The difference between the 1998–2007 and 1958–1967 decadal averages in this GFDL-MOM025 simulation reveals that the subsurface coastal ocean waters, averaged between 200 and 700 m depth, have warmed by >0.5°C from 10°W westward to 180°W (Figures 2a and 2b). The warming is strongest (>1.5°C) along the western side of the Peninsula where the Antarctic Slope Front is weak. Elsewhere along the coastline there is little temperature change at these depths, and offshore waters are characterized by cooling of <0.4°C that is commonly associated with offshore change in Ekman pumping [e.g., *Fyfe et al.*, 2007]. Around much of the coastline the coastal currents have strengthened, except in the regions with intense subsurface warming (Figures 2c and 2d). Within 200 km of the coastline from 10°W westward to 180°W and between 200 m and 700 m depth the net heat content
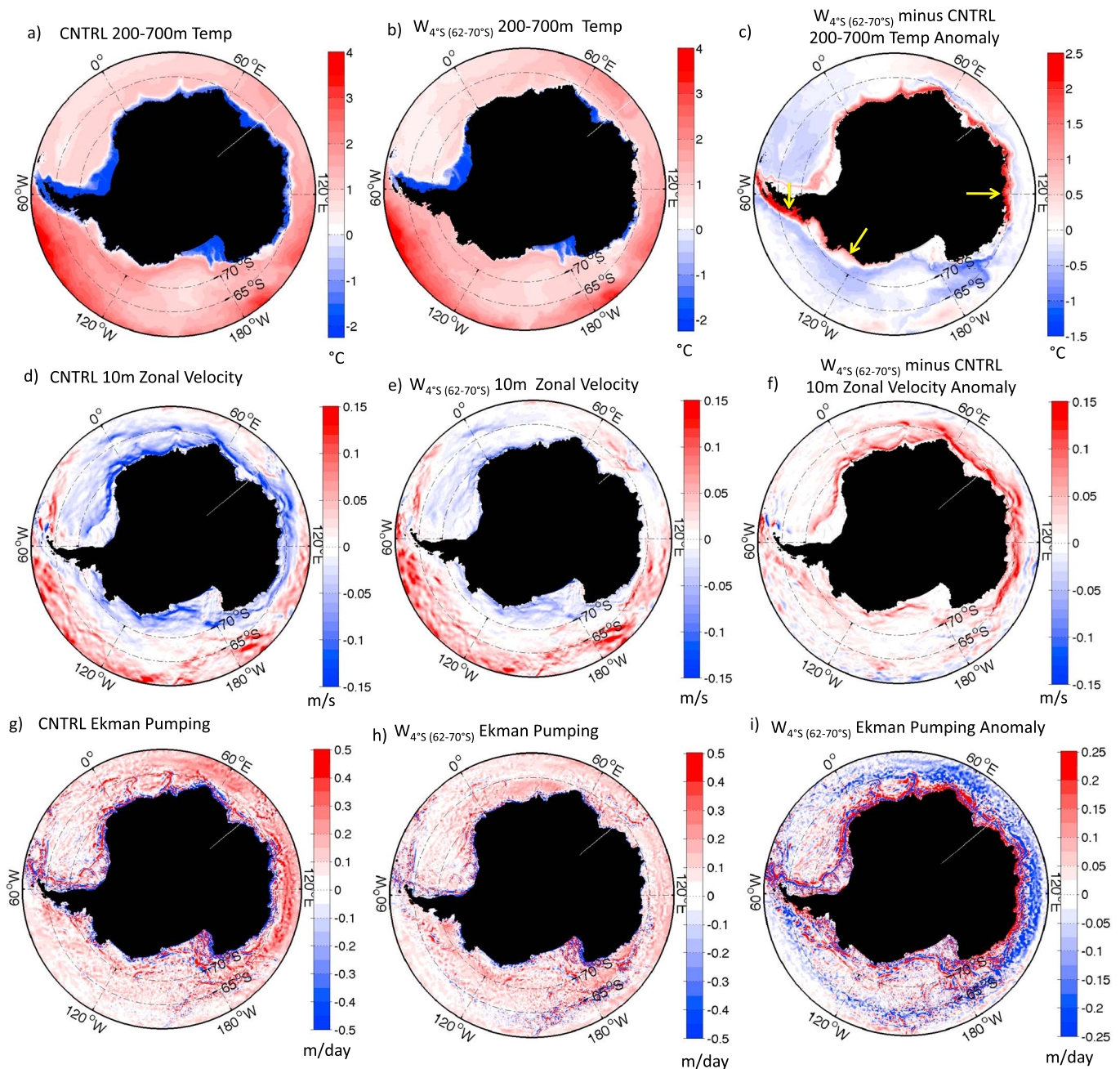
Figure 3. GFDL-MOM025 response $W_{4°S\ (62°S-70°S)}$ wind shift. Ocean temperature (°C) averaged between 200 and 700 m depth in (a) CNTRL, (b) $W_{4°S\ (62°S-70°S)}$, and (c) $W_{4°S\ (62°S-70°S)}$ minus CNTRL. Ocean zonal velocity (m/s) at 10 m depth in (d) CNTRL, (e) $W_{4°S\ (62°S-70°S)}$, and (f) $W_{4°S\ (62°S-70°S)}$ minus CNTRL. Note that the predominantly meridional velocities along the Antarctic Peninsula are not shown here but are similarly affected by the wind perturbation. Note also that the zonal velocity structures are weaker but remain consistent when depth averaged over the upper 700 m. Surface vertical velocities (m/day, positive upward) due to Ekman pumping determined from ocean surface stress in (g) CNTRL, (h) $W_{4°S\ (62°S-70°S)}$, and (i) $W_{4°S\ (62°S-70°S)}$ minus CNTRL. All values are averaged 11–20 years after the wind perturbation is initiated. Yellow arrows in Figure 3c indicate analysis regions for Figure 4.

change is 6.71×10^{20} J. If this heat were exclusively used to melt grounded land ice (assuming that the grounded ice remains static, and the resulting water mass enters the ocean), then the associated global sea level rise would be 5.5 mm.

The relative importance of the different atmospheric trends and the mechanisms by which they drive a warming of subsurface Antarctic ocean temperatures are difficult to disentangle, requiring multiple single-forcing experiments and an assumption of linearity in a highly nonlinear system. Despite this challenge, features
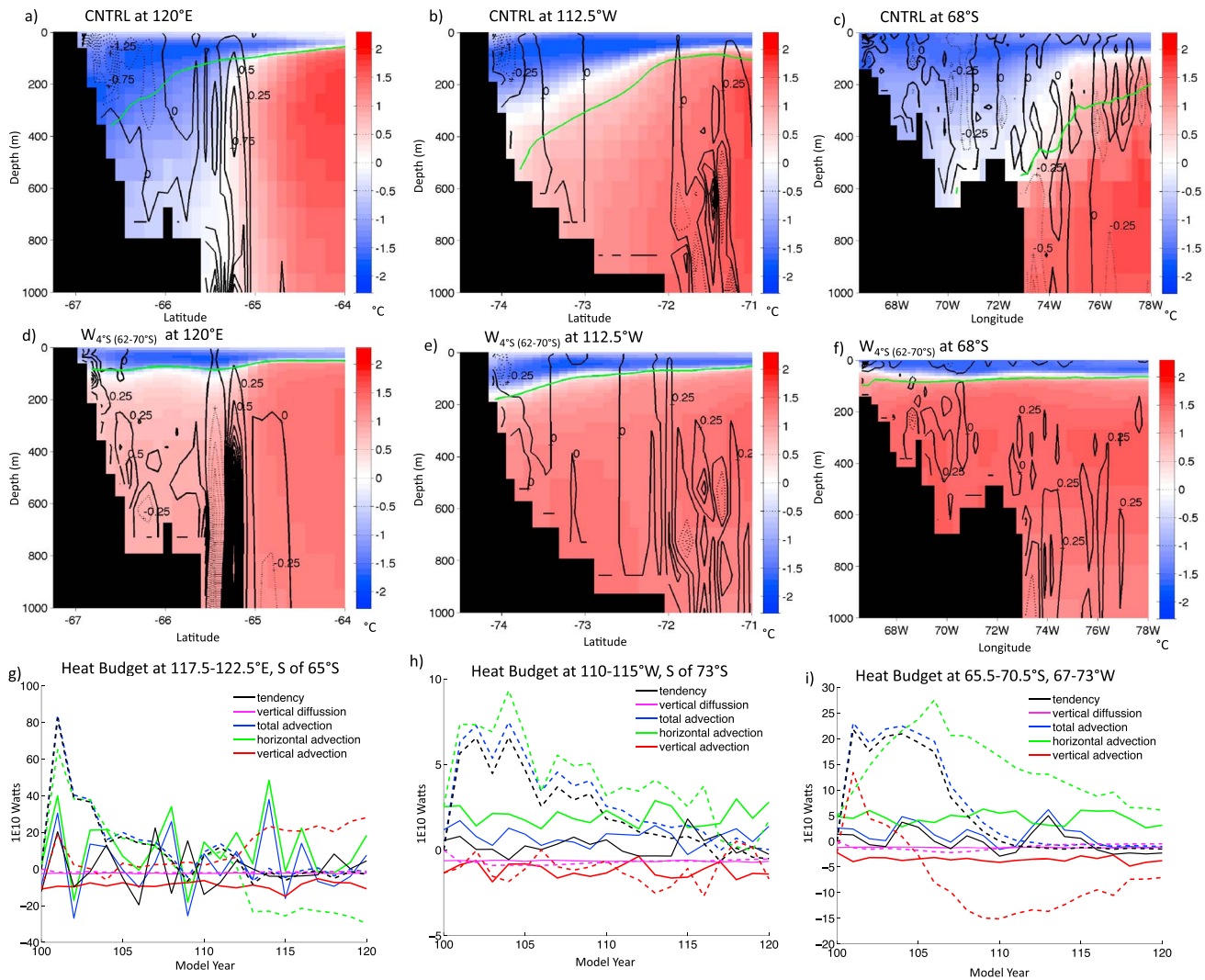
Figure 4. Response to $W_{4°S\ (62°S–70°S)}$ wind shift at 120°E (Wilkes Glacier), 112.5°W (Amundsen Sea), and 68°S (Fallieres coast). Temperature (°C; color shading) and vertical velocity (black contours at 0.25×10^{-5} m/s intervals, solid lines are upward, and dashes are downward flows) averaged 11–20 years after initial wind perturbation in (a–c) CNTRL and (d–f) $W_{4°S\ (62°S–70°S)}$. The green contour line shows the position of the 1027.6 kg/m^3 isopycnal. (g–i) Non-negligible annual mean heat budget components (10^{10} Watts) in CNTRL (lines) and $W_{4°S\ (62°S–70°S)}$ (dashes) at each location. All values are averaged over regions 5° wide. See supplementary materials for details on the heat budget calculations.

of the subsurface coastal warming response suggest that the Southern Annular Mode trend is playing a key role. First, the warming extends to greater depths than expected in response to the Antarctic Peninsula air temperature trend [*Meredith and King*, 2005]. Second, the warming is strongest where the Southern Annular Mode trend has reduced the easterly wind stress (Figures 2e and 2f) and reduced the downward Ekman pumping anomalies directly offshore (Figures 2g and 2h). However, the influence of the increased net freshwater flux (i.e., precipitation minus evaporation) in many coastal regions, particularly on the western side of the Antarctic Peninsula (Figures 2i and 2j), might also be of importance.

3.2. Idealized Wind Forcing Response

The first-order characteristics of the Antarctic coastal ocean response to the idealized wind forcing scenarios are captured in the $W_{4°S\ (62°S–70°S)}$ simulation, wherein the near surface winds between 62°S and 70°S are shifted 4°S. In less than 20 years of this forcing the Antarctic coastal waters, averaged between 200 m and 700 m depth, warm by over 0.5°C from 130°E westward to 110°W, with warming in excess of 2.5°C along the western side of the Antarctic Peninsula (Figures 3a, 3b, and 3c). The warming is coincident with a weakening of the zonal coastal
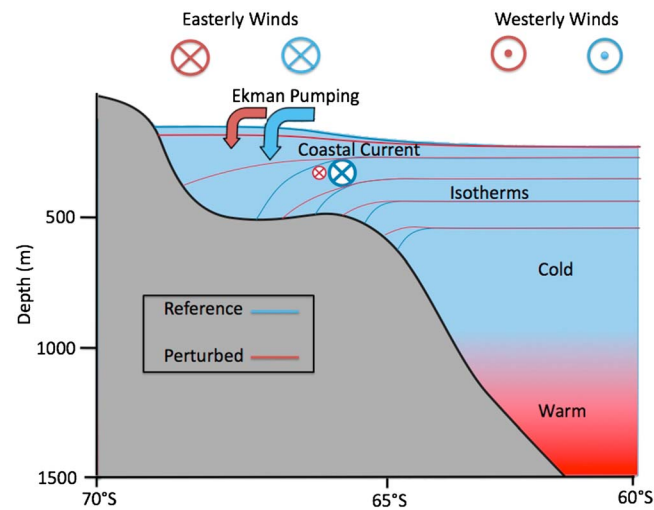
Figure 5. Schematic of Antarctic coastal ocean response to a poleward wind shift. Isotherms (lines), zonal winds, Ekman pumping (arrows), and coastal currents are shown in blue for the CNTRL case and in red for a poleward wind shift. The wind shift decreases dynamic sea surface height along the coast and flattens the isotherms, which are generally well aligned with isopycnals in this region. The speed of the coastal current decreases, and the boundary between the cold and fresh surface water near the coast and the warmer layer below moves upward.

currents by >50% in most regions (Figures 3d, 3e, and 3f), and a strong reduction in the downward coastal Ekman pumping (Figures 3g, 3h, and 3i). Within 200 km of the Antarctic coastline between 200 and 700 m depth the net heat content change is 3.54×10^{21} J, which is enough energy to melt roughly 1×10^{16} kg of ice. If exclusively used to melt grounded ice (assuming no feedback on ice dynamics), this heat would raise global sea level by 29 mm. If vertical mixing brought even a fraction of this heat to the near surface it could also dramatically reduce sea ice concentrations, with further impacts on local air-sea fluxes [*Whitworth et al.*, 1998; *Mathiot et al.*, 2012]. However, there is little change (<10%) in the sea ice concentration near the Antarctic coastline in response to the wind forcing (Figure S4), and as discussed below, ocean heat tendency terms associated with changes in sea ice coverage are small.

This pattern of near circumpolar warming of the subsurface coastal water and weakened coastal currents is closely reproduced in all GFDL-MOM025 idealized forcing scenarios that include a poleward wind shift (Figures S5 and S6). When the wind shift is extended poleward to span 62°S–80°S, warm water anomalies penetrate deeper into the Weddell and Ross seas via submarine troughs (compare Figures S5d and S5e) known to facilitate transport across the continental shelf [*Hellmer et al.*, 2012]. In contrast, for an isolated wind strengthening scenario without a poleward shift, most of the coastal boundary undergoes only mild (<0.25°C) cooling (Figure S5c) and relatively little change in coastal currents (Figure S6c).

When viewed as a function of depth and distance from the coastline in the Amundsen Sea (120°W), Wilkes Glacier (112°E), and Fallieres coast (68°S), a consistent temperature and vertical velocity response pattern is identified (Figures 4a–4f). The wind shift shoals the Antarctic Slope Front, increasing the subsurface temperatures by as much as 4°C across the continental shelf, shallowing isopycnals and substantially reducing or even reversing the predominantly downward vertical velocities across the continental shelf. A decomposition of the subsurface ocean heat budget at each location shows that most of the warming occurs within 5 years and is caused by horizontal and vertical advection tendencies explicitly resolved by the model (Figures 4g, 4h, and 4i). Note that the heat transport diagnostics include the effects of transients (e.g., mesocale eddies) as part of the heat tendency diagnostics calculated online. Heating tendencies associated with changes in buoyancy forcing (e.g., brine rejection and freshwater input) and those due to parameterized mixing associated with dense water formation remain small. This vertical velocity, isopycnal, and heat budget response are consistent in the coastal warming regions across all of the idealized GFDL-MOM025 wind forcing simulations.

4. Discussion

Pioneers of oceanography attributed the cold fresh subsurface waters observed on the Antarctic continental shelf to downwelling forced by a shoreward Ekman transport in the surface layers [*Gill*, 1973; *Sverdrup*, 1953]. The same dynamic principles can explain the simulated subsurface Antarctic coastal warming response to projected Southern Annular Mode wind trends (Figure 5). A poleward wind shift decreases the onshore Ekman transport and decreases the associated downward Ekman pumping near the coast. In turn, there is a decrease in sea level around the coastline [*Frankcombe et al.*, 2013] and a decrease in the slope of isopycnals.

SPENCE ET AL.   4608

In such a case, the meridional pressure gradient weakens, the speed of the coastal current decreases, and the boundary between the cold fresh surface water near the coast, and the warmer layer below, moves upward.

Our ocean model simulations demonstrate that a poleward wind shift at the latitudes of the Antarctic Peninsula leads to an intense and rapid advective warming of subsurface Antarctic coastal waters. This warming is associated with a weakened Antarctic Slope Front, weakened coastal currents, and upward vertical velocity anomalies on the continental shelf. Coarse resolution (i.e., >1° grid) model studies also identified subsurface warming around Antarctica in 21st century greenhouse gas scenarios, with a focus on warming associated with large-scale changes in the Southern Ocean, rather than the Antarctic coastal current described here [*Yin et al.*, 2011; *Gillet et al.*, 2011]. Our results highlight the need for ocean model grid resolution sufficiently fine to represent the Antarctic coastal current, and for winds of sufficient resolution to affect the coastal Ekman dynamics that are fundamental to the mechanism of subsurface ocean warming identified here.

There are many observed features of the Antarctic coastal environment that are not included in our simulations that warrant further consideration. Two prominent features are katabatic winds [*Mathiot et al.*, 2012], which are poorly represented in the atmospheric forcing used here, and changes in surface freshwater fluxes, especially due to enhanced glacial runoff [*Rintoul*, 2007; *Durack and Wijffels*, 2010]. We also note that while Ekman fluxes are a key determinant of Antarctic coastal isopycnal slopes, they are not the only factor [*Baines*, 2009]. In particular, mesoscale eddies have been shown in idealized studies to play a key role in setting the stratification across the Antarctic Slope Front [*Stewart and Thompson* [2013]; *Nøst et al.* [2011]; *Dinniman et al.* [2011]]. However, there are currently no realistic global ocean climate simulations capable of resolving the baroclinic Rossby radius on the Antarctic continental shelf, which requires finer than 1/16° horizontal resolution [*Hallberg*, 2013]. Further, regional ocean-sea ice-ice shelf model studies have not found a simple relationship between wind stress forcing and ice shelf melting [*Dinniman et al.*, 2012].

The stability of Antarctic ice sheets and their role in sea level rise in past and future climates remains highly uncertain. However, there is growing evidence that Antarctic glacial ice sheets are rapidly losing mass and may become unstable, particularly where warmer ocean water interacts with ice sheet grounding lines [*Fogwill et al.*, 2014; *Favier et al.*, 2014; *Joughin et al.*, 2014]. Given 21st century projections of the Southern Annular Mode and the mechanism outlined here by which it can intensely warm subsurface Antarctic coastal waters, current projections for global sea level rise may be significantly underestimated.

References

Baines, P. (2009), A model for the structure of the Antarctic Slope Front, *Deep Sea Res., Part II*, 56, 859–873.
Bintanja, R., G. van Oldenborgh, S. Drijfhout, B. Wouters, and C. Katsman (2013), Important role for ocean warming and increased ice-shelf melt in Antarctic sea-ice expansion, *Nat. Geosci.*, 6, 376–379.
Chapman, W., and J. Walsh (2007), A synthesis of Antarctic temperatures, *J. Clim.*, 20, 4096–4117.
Chavanne, C. P., K. Heywood, K. Nicholls, and I. Fer (2010), Observations of the Antarctic Slope Undercurrent in the southeastern Weddell Sea, *Geophys. Res. Lett.*, 37, L13601, doi:10.1029/2010GL043603.
Codron, F. (2005), Relation between annular modes and the mean state: Southern Hemisphere summer, *J. Clim.*, 18, 320–330.
Codron, F. (2007), Relation between annular modes and the mean state: Southern Hemisphere winter, *J. Atmos. Sci.*, 64, 3328–3339.
Delworth, T. L., et al. (2012), Simulated climate and climate change in the GFDL CM2.5 high-resolution coupled climate model, *J. Clim.*, 25, 2755–2781.
Dinniman, S., J. Klinck, and W. Smith (2011), A model study of Circumpolar Deep Water on the West Antarctic Peninsula and Ross Sea continental shelves, *Deep Sea Res., Part II*, 58, 1508–1523.
Dinniman, M., J. Klinck, and E. Hofmann (2012), Sensitivity of Circumpolar Deep Water transport and ice shelf basal melt along the West Antarctic Peninsula to changes in the winds, *J. Clim.*, 25, 4799–4816.
Durack, P. J., and S. Wijffels (2010), Fifty-year trends in global ocean salinities and their relationship to broad-scale warming, *J. Clim.*, 23, 4342–4362.
Favier, L., G. Durand, S. L. Cornford, G. H. Gudmundsson, O. Gagliardini, F. Gillet-Chaulet, T. Zwinger, A. J. Payne, and A. M. Le Brocq (2014), Retreat of Pine Island glacier controlled by marine ice-sheet instability, *Nat. Clim. Change*, 4, 117–121.
Fogwill, C., C. S. M. Turney, K. J. Meissner, N. R. Golledge, P. Spence, J. L. Roberts, M. England, R. T. Jones, and L. Carter (2014), Testing the sensitivity of the East Antarctic Ice Sheet to Southern Ocean dynamics: Past changes and future implications, *J. Quat. Sci.*, 29, 91–98.
Frankcombe, L., P. Spence, A. Hogg, M. England, and S. Griffies (2013), Sea level changes forced by Southern Ocean winds, *Geophys. Res. Lett.*, 40, 5710–5715, doi:10.1002/2013GL058104.
Fyfe, J. C., O. Saenko, K. Zickfeld, M. Eby, and A. Weaver (2007), The role of poleward intensifying winds on Southern Ocean warming, *J. Clim.*, 20, 5391–5400.
Gill, A. E. (1973), Circulation and bottom water production in the Weddell Sea, *Deep Sea Res., Oceanogr. Abstr.*, 20, 111–140.
Gillet, N. P., V. Arora, K. Zickfeld, S. Marshall, and W. Merryfield (2011), Ongoing climate change following a cessation of carbon dioxide emissions, *Nat. Geosci.*, 4, 83–87.
Griffies, S. M., et al. (2009), Coordinated Ocean-ice Reference Experiments (COREs), *Ocean Modell.*, 26, 1–46.
Hallberg, R. (2013), Using a resolution function to regulate parameterizations of oceanic mesoscale eddy effects, *Ocean Modell.*, 72, 92–103.

Hellmer, H. H., F. Kauker, R. Timmermann, J. Determann, and J. Rae (2012), Twenty-first-century warming of a large Antarctic ice-shelf cavity by a redirected coastal current, *Nature*, *485*, 225–228.

Jacobs, S. S. (1991), On the nature and significance of the Antarctic Slope Front, *Mar. Chem.*, *35*, 9–24, doi:10.1016/S0304-4203(09)90005-6.

Joughin, I., B. Smith, and B. Medley (2014), Marine ice sheet collapse potentially under way for the Thwaites glacier basin, West Antarctica, *Science*, *344*, 735–738.

Large, W. G., and S. Yeager (2009), The global climatology of an interannually varying air-sea flux data set, *Clim. Dyn.*, *33*, 341–364.

Marshall, G. (2003), Trends in the Southern Annular Mode from Observations and Reanalyses, *J. Clim.*, *16*, 4134–4143.

Mathiot, P., N. Jourdain, B. Bernier, H. Gallee, J. M. Molines, J. Le Sommer, and T. Penduff (2012), Sensitivity of coastal polynyas and high salinity shelf water production in the Ross Sea, Antarctica, to the atmospheric forcing, *Ocean Dyn.*, *62*, 701–723.

Mayewski, P. A., et al. (2009), State of the Antarctic and Southern Ocean Climate System, *Rev. Geophys.*, *47*, RG1003, doi:10.1029/2007RG000231.

Mazloff, M. R., P. Heimbach, and C. Wunsch (2010), An eddy-permitting Southern Ocean state estimate, *J. Phys. Oceanogr.*, *40*, 880–899.

Meredith, M. P., and J. King (2005), Rapid climate change in the ocean west of the Antarctic Peninsula during the second half of the 20th century, *Geophys. Res. Lett.*, *32*, L19604, doi:10.1029/2005GL024042.

Nøst, O. A., M. Biuw, V. Tverberg, C. Lydersen, T. Hattermann, Q. Zhou, L. H. Smedsrud, and K. M. Kovacs (2011), Eddy overturning of the Antarctic Slope Front controls glacial melting in the Eastern Weddell Sea, *J. Geophys. Res.*, *116*, C11014, doi:10.1029/2011JC006965.

Pritchard, H. D., and D. G. Vaughan (2007), Widespread acceleration of tidewater glaciers on the Antarctic Peninsula, *J. Geophys. Res.*, *112*, F03S29, doi:10.1029/2006JF000597.

Pritchard, H. D., S. Ligtenberg, H. Fricker, D. Vaughan, M. van den Broeke, and L. Padman (2012), Antarctic ice-sheet loss driven by basal melting of ice shelves, *Nature*, *484*, 502–505.

Rignot, E., and S. Jacobs (2002), Rapid bottom melting widespread near Antarctic ice sheet grounding lines, *Science*, *296*, 2020–2023.

Rignot, E., G. Casassa, P. Gogineni, W. Krabill, A. Rivera, and R. Thomas (2004), Accelerated ice discharge from the Antarctic Peninsula following the collapse of Larsen B ice shelf, *Geophys. Res. Lett.*, *31*, L18401, doi:10.1029/2004GL020697.

Rignot, E., J. Bamber, M. van den Broeke, C. Davis, Y. Li, W. van de Berg, and E. van Meijgarrd (2008), Recent Antarctic ice mass loss from radar interferometry and regional climate modeling, *Nat. Geosci.*, *1*, 106–110.

Rintoul, S. R. (2007), Rapid freshening of Antarctic Bottom Water formed in the Indian and Pacific oceans, *Geophys. Res. Lett.*, *34*, L06606, doi:10.1029/2006GL028550.

Schoof, C. (2007), Ice sheet grounding line dynamics: Steady states, stability, and hysteresis, *J. Geophys. Res.*, *112*, F03S28, doi:10.1029/2006JF000664.

Smedsrud, L. H., A. Jenkins, D. Holland, and O. Nøst (2006), Modeling ocean processes below Fimbulisen, Antarctica, *J. Geophys. Res.*, *111*, C01007, doi:10.1029/2005JC002915.

Spence, P., E. van Sebille, O. Saenko, and M. England (2014), Using Eulerian and Lagrangian approaches to investigate wind-driven changes in the Southern Ocean abyssal circulation, *J. Phys. Oceanogr.*, *44*, 662–675.

Stewart, A., and A. Thompson (2013), Connecting Antarctic cross-slope exchange with Southern Ocean overturning, *J. Phys. Oceanogr.*, *43*, 1453–1471.

Sverdrup, H. (1953), The currents off the coast of Queen Maude Land, *Norw. J. Geogr.*, *14*, 1–4.

Swart, N. C., and J. Fyfe (2012), Observed and simulated changes in the Southern Hemisphere surface westerly wind-stress, *Geophys. Res. Lett.*, *39*, L16711, doi:10.1029/2012GL052810.

Thompson, D. W., and S. Solomon (2002), Interpretation of recent Southern Hemisphere climate change, *Science*, *296*, 895–899.

Thompson, D. W. J., S. Solomon, P. J. Kushner, M. H. England, K. M. Grise, and D. J. Karoly (2011), Signatures of the Antarctic ozone hole in Southern Hemisphere surface climate change, *Nat. Geosci.*, *4*, 741–749.

Turner, J., S. Colwell, G. J. Marshall, T. A. Lachlan-Cope, A. M. Carleton, P. D. Jones, V. Lagun, P. A. Reid, and S. Iagovkina (2005), Antarctic climate change during the last 50 years, *Int. J. Climatol.*, *25*, 279–294.

Wåhlin, A. K., X. Yuan, G. Björk, and C. Nohr (2010), Inflow of warm Circumpolar Deep Water in the Central Amundsen Shelf, *J. Phys. Oceanogr.*, *40*, 1427–1434.

Whitworth, T., A. Orsi, S. Kim, and W. Nowlin (1998), Water masses and mixing near the Antarctic Slope Front, in *Ocean, Ice, and Atmosphere: Interactions at the Antarctic Continental Margin*, Antarct. Res. Ser., vol. 75, edited by S. S. Jacobs and R. F. Weiss, pp. 1–27, AGU, Washington, D. C.

Yin, J., J. Overpeck, S. Griffies, A. Hu, J. Russell, and R. Stouffer (2011), Different magnitudes of projected subsurface ocean warming around Greenland and Antarctica, *Nat. Geosci.*, *4*, 524–528.

Zheng, F., J. Li, R. Clark, and H. Nnamchi (2013), Simulation and projection of the Southern Hemisphere Annular Mode in CMIP5 models, *J. Clim.*, *26*, 9860–9879.